22 Stars notes 2019/10/18 - Fri - CNO burning, upper MS core convection

22.1 Upper MS central T continued

Can solve for uppor main sequence central T by putting in $R(M)$ roughly from virial argumentns

$$kT_c \simeq \frac{GMm_p\mu}{R}$$

Since we found for the sun $T_7 \approx 2$ let's re-expand at $T_7 = 2$. Then $\nu = 19$ and $f = f(T_7 = 2)(T_7/2)^{19}$ so that

$$L_{nuc} = L_{rad}$$

or

$$\epsilon M = L_{rad}$$

gives

$$\frac{M^2}{R^3} 5 \times 10^{58} \frac{1}{T_7^{2/3}} (1.3 \times 10^{-25}) \left(\frac{T_7}{2}\right)^{19} = L_\odot M^3$$

Solving this equation using the above virial relation gives

$$T_7 \approx 1.83 \left(\frac{M}{M_\odot}\right)^{4/21} \approx 1.83 \left(\frac{M}{M_\odot}\right)^{1/5}$$

Thus the central temperature of a CNO burning star is nearly independent of the stellar mass.

Now to get R and $T_{\rm eff}$,

$$R \propto \frac{M}{T_c} \propto \frac{M}{M^{1/5}} \propto M^{0.8}$$

and

$$L \propto T_{eff}^4 R^2 \quad \Longrightarrow \quad T_{\rm eff}^4 \propto \frac{L}{R^2}$$

thus

$$T_{eff}^4 \propto \frac{M^3}{M^{1.6}} \propto M^{1.4}$$

so that

$$T_{eff} \propto M^{0.34}$$

so from 1-10 $M_\odot$ there is only a factor of 2 change in T_{eff} while L varies by 1000.

Refer to figures below, also MESA paper 1 fig 22 and 29. We see that this is good up to about 10 $M_\odot$. It gets modified then as you continue to go up in mass due to photons becoming important in the pressure. Note on lifetimes: The high mass stars are done before the low mass stars even start burning. very short lifetimes.

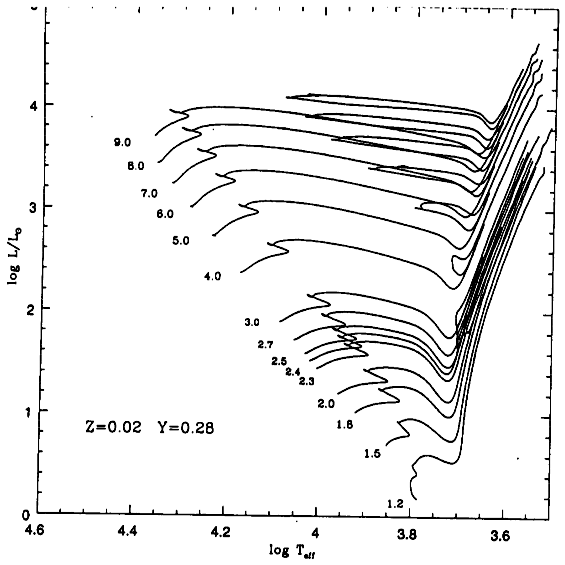

FIG. 1.—Evolutionary tracks for $Z = 0.02$, $Y = 0.28$

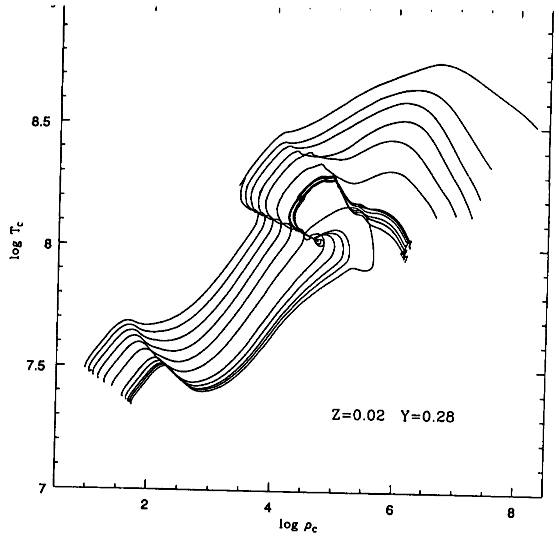

FIG. 5.—Evolution of the central temperature vs. the central density for $Z = 0.02$ and $Y = 0.28$.

PROPERTIES OF THE MODELS WITH $Z = 10^{-3}$, $Y = 0.23$

M ($M_\odot$) (1)	Δt_H (Myr) (2)	M_H^{cc} ($M_\odot$) (3)	He_{sur}^{1du} (4)	log L_{tip}^{RGB} (5)	M_{He}^1 ($M_\odot$) (6)	Δt_{He} (Myr) (7)	M_{He}^2 ($M_\odot$) (8)	He_{sur}^{2du} (9)	M_{He}^3 ($M_\odot$) (10)
1.2.....	3267	0.103	0.253	3.343	0.491				
1.5.....	1502	0.141	0.250	3.331	0.488	97.4	0.558	0.250	0.571
1.8.....	873	0.241	0.247	3.298	0.482	95.7	0.575	0.253	0.587
2.0.....	659	0.321	0.246	3.152	0.456	104	0.580	0.246	0.592
2.1.....	582	0.358	0.245	2.637	0.387	144	0.564	0.245	0.579
2.2.....	514	0.395	0.244	2.510	0.350	160	0.575	0.244	0.588
2.3.....	462	0.433	0.244	2.402	0.339	152	0.592	0.244	0.609
2.4.....	412	0.472	0.243	2.369	0.339	135	0.615	0.243	0.629
2.5.....	373	0.511	0.241	2.372	0.346	118	0.630	0.241	0.644
2.7.....	309	0.581	0.236	2.412	0.364	93.8	0.674	0.236	0.687
3.0.....	240	0.686	0.233	2.504	0.398	68.1	0.741	0.235	0.751
4.0.....	127	1.065	0.230	2.845	0.526	29.0	0.988	0.269	0.853
5.0.....	78.9	1.425	0.230	3.132	0.672	16.1	1.257	0.299	0.920
6.0.....	54.5	1.822	0.230	3.464	0.809	10.0	1.504	0.317	0.991
7.0.....	40.6	2.202	0.230	3.597	1.013	7.2	1.776	...[a]	
9.0.....	26.2	3.071	0.230	4.025	1.442	3.6	2.392	...[b]	

[a] Off-center C burning.

22.2 Structure of Upper MS Star - CNO makes a convective core

Due to the strong T dependence, the burning is very centrally concentrated and so $L(r) \approx L$ very far inside the star. To figure this out we should look at the gradient $d\ln T/d\ln P$ and see if it can set off convection. The Criterion for convection

$$\frac{d\ln T}{d\ln P} > \frac{2}{5}$$

for ideal gas. The flux is

$$F = -\frac{4}{3}\frac{ac}{\kappa\rho}T^3\frac{dT}{dr}$$

and

$$\frac{dP}{dr} = -\rho g$$

so that we get

$$\frac{d\ln T}{d\ln P} = \frac{P_{tot}}{aT^4}\frac{3}{4}\frac{\kappa}{c}\frac{L(r)}{4\pi G m(r)}$$

See that in the limit of a δ function ϵ you alway get a convective core as the above is infinite at the center. Rewriting somewhat

$$\frac{d\ln T}{d\ln P} = \frac{P_{tot}}{aT^4}\frac{3}{4}\frac{L(r)}{L_{Edd}}\frac{M}{m(r)}$$

so we want to know how far out does the convection go?

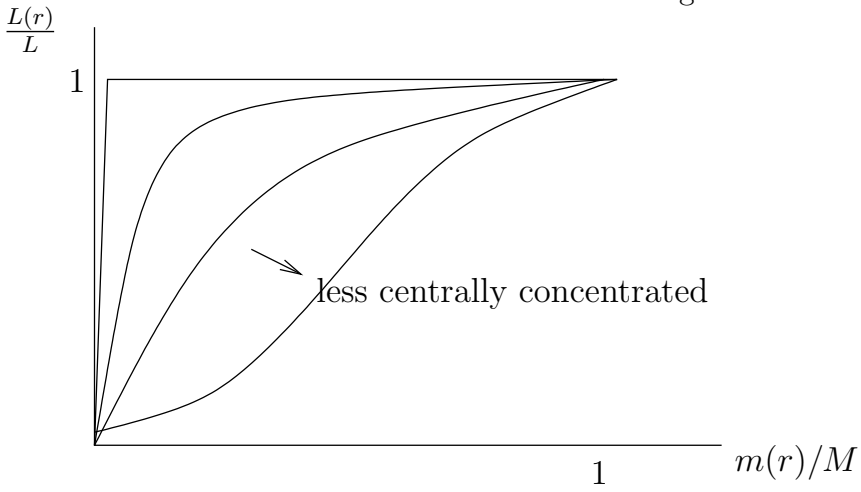

If we ask with the delta function, how far out do we need to go to get out of convection? From before we had

$$\frac{P_{tot}}{P_{rad}} = 2600(M_\odot/M)^2$$

and

$$\frac{L}{L_{Edd}} = 4\times 10^{-5}(M/M_\odot)^2$$

so then asking where

$$\frac{d\ln T}{d\ln P} = 0.1\frac{M}{m(r)} > \frac{2}{5}$$

gives

$$m(r) < \frac{1}{4}M$$

So if the energy is generated in less than about a quarter of the mass, there will be a convective core.

So the cores of massive stars convect, but the outer layers become stable and so the heat transport is still limited by radiative diffusion. That is, the radius and M-L relation are still determined by radiative diffusion. So then the structure is:

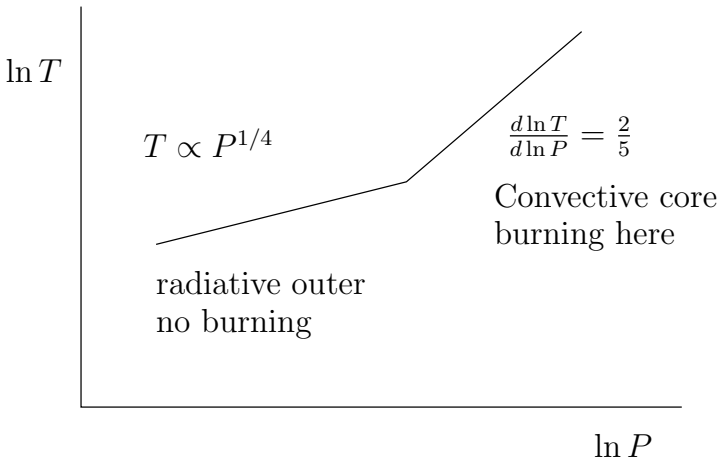

Making a table including upper and lower main sequence stars

$M/M_\odot$	T_7	$q_c = M_{conv}/M$	$q_{env} = M_{conv,env}/M$
60	3.9	0.73	0
15	3.3	0.4	0
5	2.64	0.23	0
1.5	1.9	0.07	0
1.0	1.5	0	0.0035
0.6	0.9	0	0.7
0.3		1	1

Note those above $1M_\odot$ are burning via CNO and those 1.0 and below are pp burning. So we can draw two pictures:

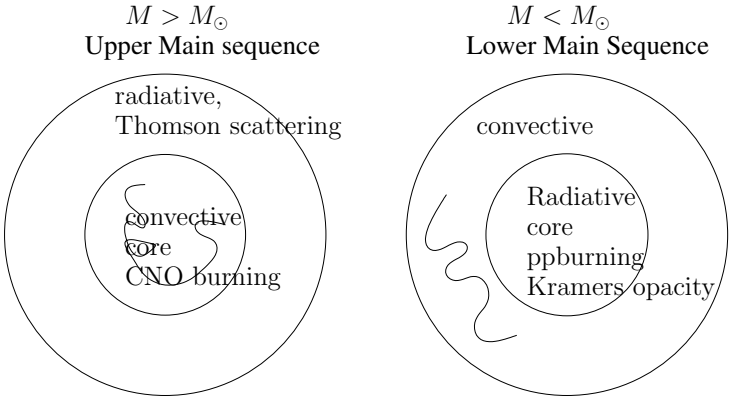

These are zero age main sequence.

Show plots of several T-ρ structures showing convection from first MESA paper fig 3.

22.3 Physical basis for two spectral parameters

at the atmosphere, the scale height is

$$H_P = \frac{kT}{\mu m_p g} \ll R$$

so then all atmospheric calculations can be done in a plane-parallel geometry. In that geometry the only parameters are $g = GM/R^2$ and the flux F leaving in erg/cm^2-sec. and the chemical abundances. We rewrite flux as

$$T_{eff} \equiv \left(\frac{F}{\sigma_{SB}}\right)^{1/4}$$

Most of what we see in spectra is variations T_{eff} and we can measure this quite well.

At the photosphere

$$\tau = 1 = \int \kappa\rho dr = \kappa y = \kappa\frac{P}{g}$$

for an ideal gas at the photosphere

$$P = \frac{\rho k T_{eff}}{\mu m_p}$$

so the number density is

$$n_{ph} \simeq \frac{m_p g}{\sigma_{Th} k_B T_{eff}}$$

for $\kappa = \kappa_{es}$ so the number density scales with gravity, the photosphere will be denser at higher gravities. Putting numbers for the Sun

$$n_{ph} \simeq 10^{16} cm^{-3} \left(\frac{10^4}{T_{eff}}\right)\left(\frac{g}{2.7\times 10^4 cm/s^2}\right)$$

Formation of spectral lines: "absorption" lines (deficits in flux) appear because photons at line wavelengeth come from shallower (cooler) depth in atmosphere. Opacity, κ, is higher for photons at line wavelength, so line photosphere ($\tau = \kappa P/g = 1$) is shallower (lower P).

22.4 Spectral Sequence for Stars

Now use the Saha equation to get some sense of the spectral types.

The sequence is O B A F G K M, hot to cool. This is an effective temperature scale. There are gradations within this O1→O10, B0→B10. increasing number is colder. Also note that in some classes not all the numbers are filled in.

Additionaly, Luminosity class: V = dwarf → I = supergiants.

Sp Type	T_{eff}	$M/M_\odot$ (ZAMS)
O3	52,000	120
O8	36,000	23
B0	30,000	17
B5	15,400	6
A0	9520	3
G0	6030	1.05
M0	3850	0.5

The luminosity classes are really indexed by g, but it is hard to really measure this value. Sets the photospheric density.

Two spectral types for really cold dwarf (fairly recent additions) L and T classes.

Even worse: the spectral locations are referred to as Early type (OB) and Late type (KM). This from an old idea of stellar evolution.

22.5 Ionization states and spectral appearance

Really determines what the spectrum "looks" like. Quantum has to be used to set the actual temperature scale. Most of the spectral classification comes from the presence/absence of different elemental features. (Based on first ionization potential)

Alkali metals (Li, Na, Mg, Al), ≤ 5 eV

– (H, C, N, O) $10 < E < 20$ eV

Noble (He, Ne) > 20 eV

Can get a sense by following a few ionization states. Follow ionization state for (First ionization potential) FIP: H - 13.6 eV, He - 24.6 eV, Na - 5.14 eV.

For Na, $\underline{Na^+ + e^- \leftrightarrow Na + \gamma}$ which gives Saha equation

$$\frac{n_{Na+} n_e}{n_{Na}} = \left(\frac{2\pi m_e kT}{h^2}\right)^{3/2} \exp\left(-\frac{E_i}{kT}\right)$$

taking the ratio for different species the prefactor cancels so can compare Na to H

$$\frac{n_{Na^+}}{n_{Na}} = \exp\left(-\frac{(E_{Na} - E_H)}{kT}\right) \frac{n_{H^+}}{n_H} = 10^7 \frac{n_{H^+}}{n_H}$$

and similarly for He

$$\frac{n_{He^+}}{n_{He}} = \exp\left(-\frac{(E_{He} - E_H)}{kT}\right) \frac{n_{H^+}}{n_H} = 6 \times 10^{-10} \frac{n_{H^+}}{n_H}$$

where the numbers are for the sun at $T = 6000$ K. so the Na is ionized but the He is not.

$n_e(cm^{-3})$	$T_{1/2}$(Na)	$T_{1/2}$(H)	$T_{1/2}$(He)
10^{13}	3090	8000	14500
10^{14}	3500	9082	16500
10^{15}	4057	10500	19000
10^{16}	4810	12450	22570

22.6 Showing some spectra

Figure 8.4 and 8.5 from Carroll and Ostlie show examples of various spectral types:

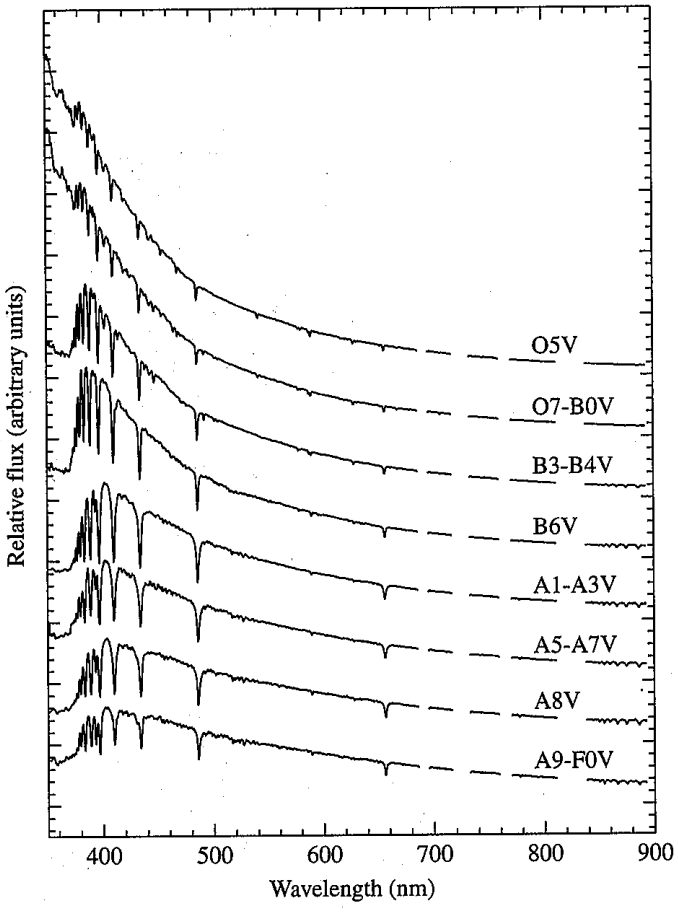

FIGURE 8.4 Digitized spectra of main sequence classes O5–F0 displayed in terms of relative flux as a function of wavelength. Modern spectra obtained by digital detectors (as opposed to photographic plates) are generally displayed graphically. (Data from Silva and Cornell, *Ap. J. Suppl.*, *81*, 865, 1992.)

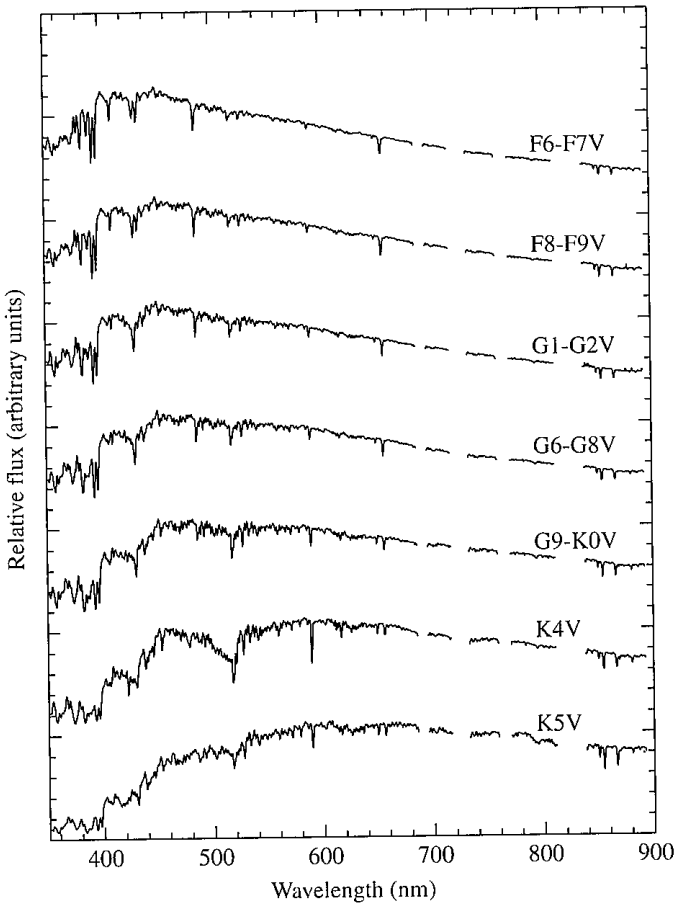

FIGURE 8.5 Digitized spectra of main sequence classes F6–K5 displayed in terms of relative flux as a function of wavelength. (Data from Silva and Cornell, *Ap. J. Suppl.*, *81*, 865, 1992.)

OB Type: All H is ionized, He is either neutral or partially ionized. at late B you start to see Balmer.

A Type: H lines, ionized Mg are present.

F Type: Mostly metal lines as most H is neutral AND all in ground state.

G and K

and finally M class

spectra for L and T class:

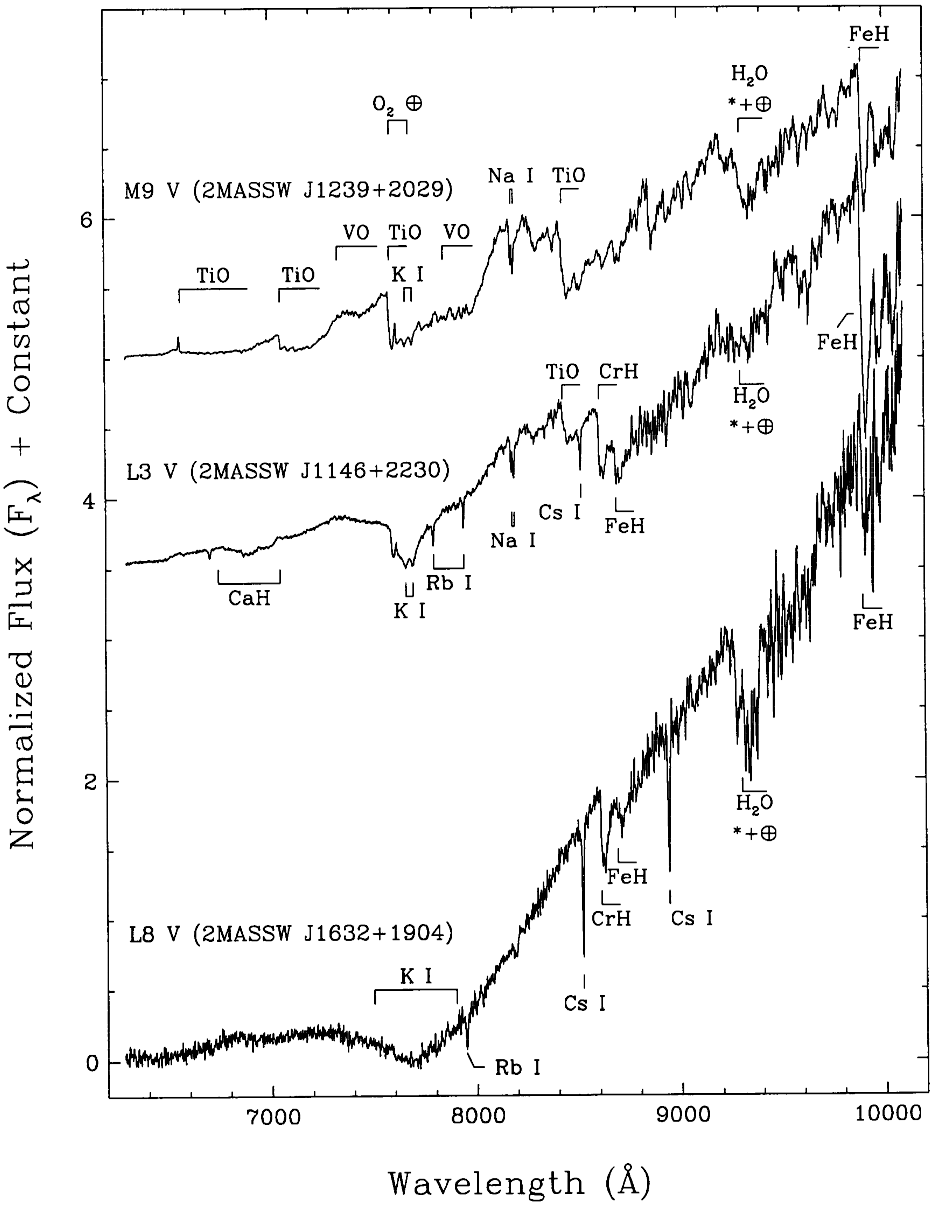

FIG. 4.—Enlarged spectra of a late-M, early- to mid-L, and late-L dwarf. Prominent features are marked. Note the absence of oxide absorption in the L dwarfs along with the dominance of alkali lines and hydride bands. Names for the 2MASS objects have been abbreviated.

dwarfs of type M7 and later, these types were refined using the VO ratio described in Kirkpatrick, Henry, & Irwin (1997b).

All dwarfs later than spectral type M9.5 are discussed in the next section, and notes on individual M9.5+ dwarfs can be found in Appendix A. Notes on other interesting objects can be found in Appendix B.

4. RESULTS FOR DWARFS COOLER THAN TYPE M9.5 V

Listed in Table 3 are all the dwarfs from Tables 1A and 2 that have spectral types cooler than M9.5 V. This includes the 2MASS dwarf discovered in Prototype Camera data (Kirkpatrick et al. 1997a), Kelu-1 discovered during the course of the proper-motion survey of Ruiz, Leggett, & Allard (1997), and the three cool dwarfs discovered by the Deep Near Infrared Survey (DENIS; Delfosse et al. 1997; Tinney, Delfosse, & Forveille 1997). Also included in the table for comparison purposes are the only two companion objects currently known with spectral types cooler than M9.5 V: GD 165B and Gl 229B. In total, 26 dwarfs have been found with post-M9.5 types, and 20 of those are from 2MASS. Optical and near-infrared finder charts for the

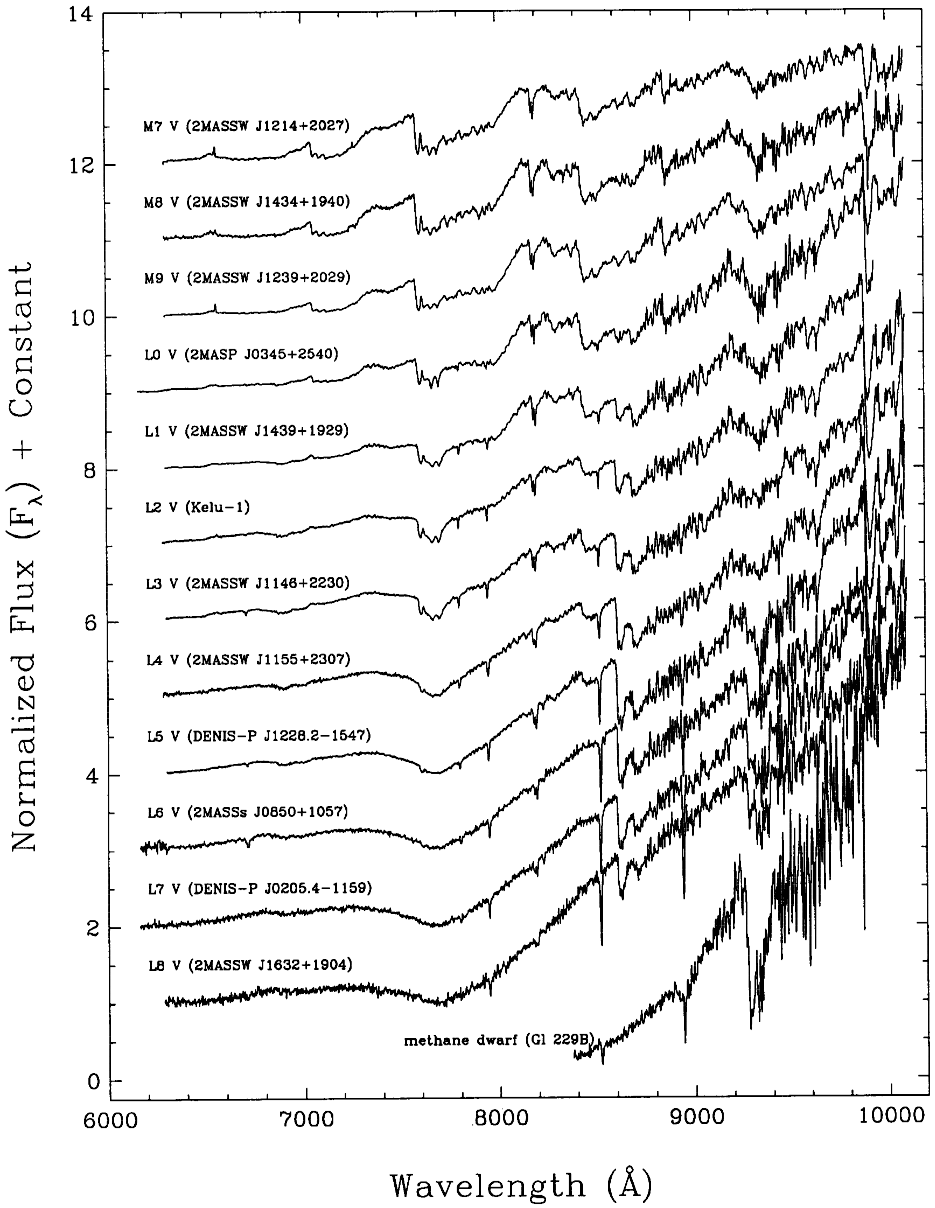

FIG. 6.—L-dwarf spectral sequence. This is a subset of the Keck LRIS data of Fig. 3, but showing only one spectrum for each subclass from L0 through L8. Also shown for comparison is the Oppenheimer et al. spectrum of Gl 229B and three late-M dwarfs from Table 1A, also taken with LRIS on Keck. Again, names for the 2MASS objects have been abbreviated.

well behaved, clearly demonstrating the fact that CrH increases strength from late M through early L, reaches peak strength at L5 V, then weakens toward the latest L types.[9] The FeH-a and FeH-b ratios show similar behavior, with FeH increasing from late M through mid-L then weakening toward the latest L types.

Because the alkalis of Figure 8 and the oxides of Figure 9 show ratios for the primary standards that monotonically increase or decrease throughout the L sequence, composite alkali-oxide ratios, which serve as more sensitive discriminants, can be devised. The values for some of these ratios are shown in Figure 11, where the primary standards are again illustrated by the large dots.

[9] As Figure 10*b* shows, the CrH-b ratio, which measures the CrH band at 9969 Å, is unusable as a spectral diagnostic in these data. This is because of the poor sensitivity of the CCD at this wavelength and because of the lack of a suitable continuum region.

definitions of spectral types L and T.

Kirkpatrick et al '99 ApJ 519, 802

TABLE 6

QUALITATIVE DEFINITIONS FOR L SUBCLASSES

Subclass (1)	Spectral Characteristics[a] (2)	Example (3)
L0	VO λλ7400, 7900 at its strongest—7800–8000 Å portion of spectrum is flat TiO λ8432 depth similar to both CrH λ8611 and FeH λ8692 TiO λ7053 present at high signal-to-noise but weak Rb I and Cs I doublets weakly visible but strengthening	2MASP J0345432+254023
L1	TiO λ8432, CrH λ8611, FeH λ8692 nearly equal strength; FeH deeper than CrH, CrH deeper than TiO VO λλ7400, 7900 weakening; 7800–8000 Å portion of spectrum slightly sloped Na I doublet weakening TiO λλ7053, 8432 weakening Rb I and Cs I doublets strengthening K I line cores broadening	2MASSW J1439284+192915
L2	TiO λ8432 much weaker than CrH λ8611 or FeH λ8692; FeH deeper than CrH K I line cores still visible and still broadening TiO λ8432 weaker and TiO λ7053 vanished VO λλ7400, 7900 weakening more: 7800–8000 portion of spectrum distinctly sloped Na I weakening; Rb I and Cs I still strengthening	Kelu-1
L3	K I still broadening with cores still weakly visible VO λ7900 barely present as slight depression in "continuum" between 7800 and 8200 Å TiO λ8432 still weakening Na I still weakening; Rb I and Cs I still strengthening	2MASSW J1146345+223053
L4	K I wings are very broad and line cores no longer visible CrH λ8611 equal in strength to FeH λ8692 VO λ7900 vanished (no depression visible at all between 7800 and 8200 Å) TiO λ8432 still weakening Na I still weakening; Rb I and Cs I still strengthening	2MASSW J1155009+230706
L5	CrH λ8611 now stronger than FeH λ8692 TiO λ8432 very weak K I region shows broad depression Na I still weakening Rb I and Cs I still strengthening; Cs I λ8521 less deep than CrH λ8611	DENIS-P J1228.2−1547
L6	TiO λ8432 barely perceptible K I region shows very broad depression FeH λλ8692, 9896 and CrH λ8611 weakening; CrH λ8611 deeper than FeH λ8692 Na I still weakening Rb I and Cs I still strengthening; Cs I λ8521 now deeper than CrH λ8611	2MASSs J0850359+105716
L7	TiO λ8432 virtually gone FeH λλ8692, 9896 and CrH λ8611 still weakening; CrH λ8611 still deeper than FeH λ8692 K I region shows very broad depression Rb I and Cs I still strengthening Na I still weakening	DENIS-P J0205.4−1159
L8	FeH λλ8692, 9896 very weak CrH λ8611 still weakening though still stronger than FeH λ8692 K I region shows very broad depression Rb I and Cs I still strengthening; Cs I λ8521 ~2 times as deep as CrH λ8611 Na I barely perceptible	2MASSW J1632291+190441

[a] Relative depths of bands refer to spectra with absolute flux calibrations (F_λ) similar to those in Figs. 7 and 8.

TABLE 11

SPECTRAL FEATURES USABLE AS L-DWARF TEMPERATURE INDICATORS

Atom or Molecule (1)	Observed Maximum (2)	Observed Disappearance (3)	Theoretical Explanation[a] (4)	Predicted Disappearance[a] (5)
TiO	~M8	~L2[b]	Condenses into $CaTiO_3$	2300–2000 K
VO	~M9	~L4	Depletes into solid VO	1700–1900 K
FeH	~L4	>L8	...[c]	...[c]
CrH	~L5	>L8	Converts into metallic CrH	~1400 K
Li I	~L6?	~L7?	Forms into LiCl	≤1400 K
CO	...	...	C becomes bound to CH_4	1200–1500 K
Rb I	≥L8	...	Forms into RbCl	≤1200 K
Cs I	≥L8	...	Forms into CsCl	≤1200 K
K I	...	...	Forms into KCl	≤1200 K
Na I[d]	...	...	Forms into NaCl	~1150 K
H_2O	...	...	Disappears into H_2O condensate	~350 K

[a] Taken from Burrows & Sharp 1999.
[b] True for all bands except the one at 8432 Å, which doesn't disappear until about L5–6.
[c] Not included in Burrows & Sharp 1999.
[d] Only a higher excitation doublet, not the ground-state doublet, is included in our spectral region. See text for discussion.